

Rapid mixing in microchannel using standing bulk acoustic waves

Cite as: Phys. Fluids 31, 122001 (2019); <https://doi.org/10.1063/1.5126259>

Submitted: 31 August 2019 . Accepted: 24 November 2019 . Published Online: 10 December 2019

Charish Pothuri, Mohammed Azharudeen, and Karthick Subramani 



[View Online](#)



[Export Citation](#)



[CrossMark](#)



AIP Conference Proceedings
FLASH WINTER SALE!
50% OFF ALL PRINT PROCEEDINGS
ENTER CODE **50DEC19** AT CHECKOUT

Rapid mixing in microchannel using standing bulk acoustic waves

Cite as: Phys. Fluids 31, 122001 (2019); doi: 10.1063/1.5126259

Submitted: 31 August 2019 • Accepted: 24 November 2019 •

Published Online: 10 December 2019



View Online



Export Citation



CrossMark

Charish Pothuri,^{1,a)} Mohammed Azharudeen,^{1,a)} and Karthick Subramani^{2,b)}

AFFILIATIONS

¹ Department of Mechanical Engineering, Shiv Nadar University, Gautam Buddha Nagar, Uttar Pradesh 201314, India

² Indian Institute of Information Technology, Design and Manufacturing, Kancheepuram, Chennai 600127, India

^{a)}**Contributions:** C. Pothuri and M. Azharudeen contributed equally to this work.

^{b)}**Electronic mail:** karthick@iitdm.ac.in

ABSTRACT

We present a technique for mixing the fluids in a microchannel using ultrasonic waves. Acoustic mixing is driven by the acoustic body force, which depends on the density gradient and speed of the sound gradient of the inhomogeneous fluid domain. In this work, mixing of fluids in a microchannel is achieved via an alternating multinode mixing method, which employs acoustic multinode standing waves of time-varying wavelengths at regular time intervals. The proposed technique is rapid, efficient, and found to enhance the mixing of fluids significantly. It is shown that the mixing time due to acoustic mixing (2–3 s) is reduced by two orders of magnitude compared to the mixing time only due to diffusion (400 s). Furthermore, we investigate the effects of the acoustic mixing on different fluid flow configurations and sound wave propagation directions as they have a direct influence on mixing time and have rarely been addressed previously. Remarkably, it is found that mixing performance is strongly dependent on the direction of the acoustic wave propagation. The acoustic field propagated parallel to the fluid-fluid interface mixes fluids rapidly (2–3 s) as compared to the acoustic field propagated perpendicular to the fluid-fluid interface (40 s).

Published under license by AIP Publishing. <https://doi.org/10.1063/1.5126259>

I. INTRODUCTION

Microscale processes have gained significant prominence in a wide variety of modern application fields during the past decade, such as biochemical production, pharmacy, and environmental and biomedical industries.^{1–7} Performing biological and chemical assays is one such process, which often involves micromixing of samples and reagents in microchannel systems, such as microfluidic lab-on-a-chip based devices.^{8,9} Mixing at such smaller length scales is quite difficult as the system is restricted to the laminar flow regime with Reynolds number <1 , unlike the macroscale flows, where instability and turbulence are responsible for mixing at a shorter timescale. At the microscale, when two fluid streams flow in parallel, mixing occurs only due to diffusion, which is ineffective as it requires longer mixing time and a very long microchannel. Hence, there is a need for novel techniques and methods for effective mixing in microfluidic systems. In the light of recent developments in microfluidic technology, two common methods of mixing have evolved, namely, passive and active mixing.^{10–12} Passive mixers do not need an

external energy source; therefore, its performance is critically coupled to flow and geometry.¹³ Grooved surfaces,¹⁴ T-shaped,¹⁵ serpentine,¹⁶ zigzag,¹⁷ etc., are good examples of passive mixers. Passive mixers need complex microchannel geometries that are challenging in fabrication and often involve a longer mixing time scale than typical microfluidic residence time, which makes this method less favorable.

Active mixing, on the other hand, employs an external energy source and thereby the mixing effect is enhanced. Active mixing methods augment the mixing performance by agitating the fluid flow with the use of typical external energy sources such as electric field,^{18–22} pressure field,^{23–26} magnetic field,^{27–31} sound field,^{32–35} and heat source.^{36,37} In the recent years, mixing enhancement using acoustic waves has gained a lot of interest in microfluidics due to easy control and high-frequency response. Steps have already been taken in the direction of mixing the fluids in a microchannel through acoustic streaming,^{38,39} bubble-based acoustic mixers,^{40,41} and surface acoustic waves (SAW) based mixers.^{42–45} However, recently, the suppression of acoustic streaming

in inhomogeneous fluids was demonstrated experimentally, and the same phenomenon was explained by using the theory of nonlinear acoustics.^{46–48} Most of the reagents that we encounter commonly in chemical and biological assays are inhomogeneous, so acoustic mixing based on acoustic streaming may not be effective. More importantly, it has been demonstrated that inhomogeneous fluids subjected to an acoustic standing wave lead to relocation of fluids to certain stable configurations under the action of nondissipative acoustic force density.^{49–51} This acoustic relocation phenomenon can serve as a promising active mixing method.

In this theoretical study, we demonstrate a novel acoustic mixing technique based on the principle of fluid-relocation in a microchannel contrary to the previous efforts based on acoustic streaming. The time-varying acoustic force density, which results from the alternating multinode (AMN) standing wave, is employed to produce more parallel laminations and strong chaotic advection in order to facilitate rapid mixing. We have shown that the mixing time due to acoustics is reduced by two orders of magnitude compared to the mixing without acoustics or only due to diffusion. It has been further demonstrated that acoustic wave propagation direction parallel to the fluid-fluid interface shows better mixing performance compared to the standing sound wave direction propagated perpendicular to the fluid-fluid interface.

II. THEORETICAL MODEL

Recent experiments demonstrated the novel phenomenon of the relocation and stabilization of inhomogeneous fluids in a microchannel when subjected to the standing acoustic wave.^{49,51} The main motive of the current work is to introduce a novel acoustic mixing method in a microchannel based on the acoustic relocation phenomenon. The fundamental idea of alternating multinode (AMN) mixing mechanism has mainly two steps: first, to increase the number of fluid-fluid interfaces or parallel

laminations by relocating the fluids using multinode standing waves. The above effectively reduces the mixing time by reducing the striation mixing length. Second, to further enhance the mixing, the number of nodes and their positions are changed periodically by altering the frequency of the standing wave to create the chaotic advection.

A. Model setup

The microchannel flow configurations considered in this study are the most commonly encountered flow configurations in microfluidics, as shown in Fig. 1. Three different flow configurations are considered, namely, 3-inlet coflow [Fig. 1(a)], 2-inlet coflow of equal width [Fig. 1(b)], and 2-inlet coflow of unequal width [Fig. 1(c)]. We use a straight, square microchannel, where the flow is established along the z-axis with a channel cross-section of width $W = 400 \mu\text{m}$ and height $H = 400 \mu\text{m}$, as sketched in Fig. 1. The channel is filled with inhomogeneous density $\rho_0(r, \tau)$ = $\rho_0^{(0)}[1 + \hat{\rho}(r, \tau)]$ and inhomogeneous speed of sound $c_0(r, \tau)$ = $c_0^{(0)}[1 + \hat{c}(r, \tau)]$, where $\hat{\rho}(r, \tau)$ and $\hat{c}(r, \tau)$ are dimensionless relative deviations away from the reference density $\rho_0^{(0)}$ and reference speed of sound $c_0^{(0)}$. In order to reduce computation time significantly, in the current work, only the 2D cross-section of the microchannel plane perpendicular to the axial flow is studied, and the same will be justified latter. Along with the different flow configurations, the direction of sound wave propagation with respect to the fluid-fluid interface is also varied, as shown in Fig. 1. The aqueous solutions of different iodixanol concentrations are used as working fluids in the study to establish the inhomogeneity in density and compressibility inside the microchannel, while maintaining an approximately constant speed of sound. The fluid properties and acoustic properties such as density, viscosity, and velocity of sound for the iodixinal aqueous solution used in this study are taken from the literature.

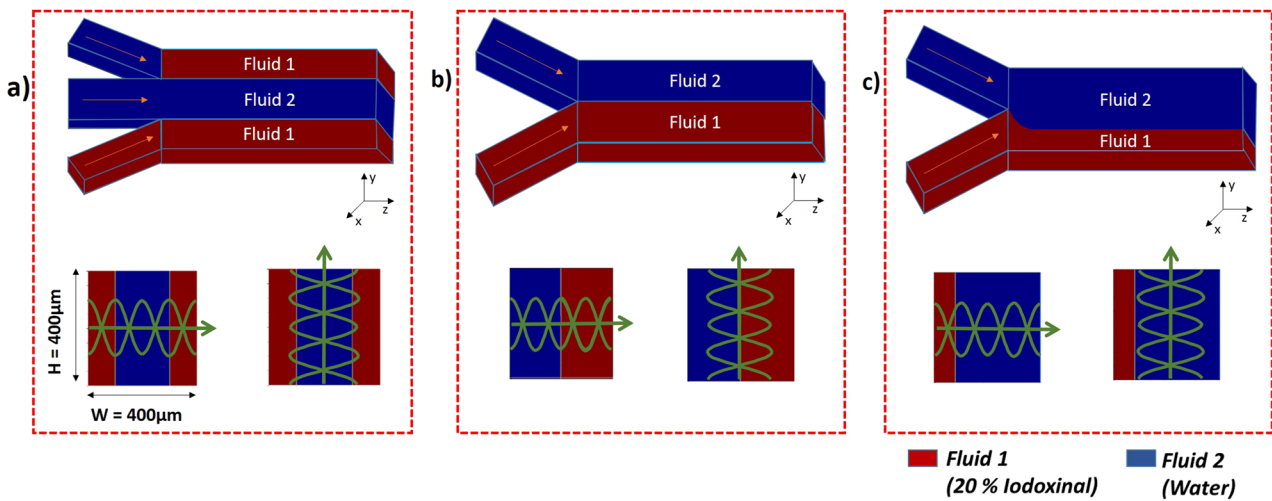


FIG. 1. 3D schematic of the microchannel flow configurations and 2D cross section (xy-plane) of the initial concentration distribution in a squared microchannel of width $400 \mu\text{m}$ and height $400 \mu\text{m}$ for: (a) 3-inlet coflow configuration, (b) 2-inlet coflow configuration of equal width, and (c) 2-inlet coflow configuration of unequal width. For different initial configurations, the sound waves are propagated parallel or perpendicular to the interface.

In our first model, as shown in Fig. 1(a), we generate 3-inlet coflow stream in which density gradient is set up by focusing central high dense (20% iodixanol, $\rho = 1110 \text{ kg/m}^3$) solution by the adjoining less dense side inlet water ($\rho = 1005 \text{ kg/m}^3$). Relative density deviation $\hat{\rho}$ is varied upto 0.1, which is well within the relevant limit, as will be discussed. The second model, as shown in Fig. 1(b) utilizes a 2-inlet coflow system of equal width with the right half of the domain width occupied with denser fluid and the rest with less dense fluid. The third model extends our previous second model with denser fluid occupying lesser width than the former within the 2-inlet microchannel, as shown in Fig. 1(c).

B. Governing equations

In this section, the governing equations employed to simulate the fluid mixing using acoustic waves are discussed. This unsteady laminar convection-diffusion flow problem is governed by the continuity equation, Navier-Stokes equation, and convection-diffusion equation. The acoustic force density f_{ac} , which is responsible for the fluid mixing, is the given input as a body force term in the right-hand side of the Navier-Stokes equation. The continuity and Navier-Stokes equations can be written as

$$\frac{\partial \rho}{\partial t} + \nabla \cdot (\rho u) = 0, \quad (1)$$

$$\begin{aligned} \rho \left(\frac{\partial u}{\partial t} \right) + \rho (u \cdot \nabla) u &= \nabla \cdot \left(-p + \nabla \cdot \mu \left(\nabla u + (\nabla u)^T \right) \right. \\ &\quad \left. - \frac{2}{3} \mu (\nabla \cdot u) I \right) + f_{ac}, \end{aligned} \quad (2)$$

where u is the fluid velocity field, p is the fluid pressure, ρ is the fluid density, μ is the fluid viscosity, and I is the identity matrix. The advection-diffusion equation takes the form,

$$\frac{\partial \phi}{\partial t} = \nabla \cdot (D \nabla \phi) - \nabla \cdot (u \phi), \quad (3)$$

where D is the diffusion coefficient and ϕ is the solute concentration field.

The following assumptions are made in our study to simplify our theoretical model. Fluid flow in the microchannel is assumed to be laminar and isothermal. The hydrostatic pressure difference due to gravity body force is negligible compared to the acoustic body force. Hence, the body force term due to gravity is neglected. The working fluid is assumed to be isotropic and Newtonian. The inhomogeneity in the fluid and acoustic properties, such as, density ρ , viscosity μ , and velocity of sound c are assumed to only vary with respect to the spatially varying solute concentration field ϕ . No-slip boundary condition for the velocity field ($u = 0$) is imposed on the microchannel boundary and no flux condition for the concentration field ($n \cdot D \nabla \phi = 0$) is imposed at the boundary. The initial velocity ($u_{t=0} = 0$) of the inhomogeneous fluids is taken as zero. The diffusivity of iodixanol D is taken as $0.9 \times 10^{-10} \text{ m}^2/\text{s}$.

C. Acoustic body force

When the inhomogeneous fluid is subjected to the acoustic field, acoustic body forces created in the flow field can relocate the inhomogeneous fluids to stable field-dependent configuration.^{49,51}

Experimentally, a high-density fluid portion in the flow field is relocated to the pressure node, and a low-density fluid portion is relocated to pressure antinode under the acoustic standing wave field.⁴⁹ This observed phenomenon can be explained using the presence of a body force called acoustic force density f_{ac} , which stems from the theory of nonlinear acoustics.⁵¹

Typically, at megahertz operating frequency range, the acoustic oscillation time scale is of order $t_{ac} \sim 1/\omega \sim 0.1 \mu\text{s}$, whereas the fluid motion due to acoustic force density takes place typically on a $10 \text{ ms}^{-1} \text{ s}$ time scale.⁵¹ This significant separation in time scales (five magnitudes slower than the acoustic time scale) leads to the possibility of splitting the problem into a slow-time-scale-acoustics ($t \sim 10 \text{ ms}$) and a fast acoustic time scale ($t \sim 0.1 \mu\text{s}$). It is shown that fast-timescale acoustics in the inhomogeneous fluids results in a second order time-averaged acoustic force density f_{ac} , acting on slow-time-scale hydrodynamics as an external driving force. This separation of timescales allows the resulting complex flows to be sufficiently described and simulated on a slower hydrodynamic time scale without the need to resolve the fast time scale of acoustic oscillations.⁵¹

In the event of inhomogeneity in the fluid with variations in density or speed of sound, the energy density E_{ac} in fluids due to the standing acoustic wave is no longer constant as in a homogeneous fluid and leads to an imbalance in the momentum-flux-density. This introduces the presence of nondissipative acoustic force density f_{ac} , which is derived from the divergence of the time-averaged momentum-flux-density tensor Π , given by⁵¹

$$f_{ac} = -\nabla \cdot \langle \Pi \rangle, \quad (4)$$

where the angled bracket denotes the time average over one oscillation period. Considering approximations to second order, the time-averaged acoustic momentum-flux-density tensor is given in terms of first-order fields by

$$\langle \Pi \rangle = \langle p_{11} \rangle I + \langle \rho_0 v_1 v_1 \rangle, \quad (5)$$

where I is the unit tensor, and the second-order mean Eulerian excess pressure p_{11} is given by the difference between the time-averaged acoustic potential and kinetic energy densities

$$\langle p_{11} \rangle = \frac{1}{2} \kappa_0 \langle p_1^2 \rangle - \frac{1}{2} \rho_0 \langle v_1^2 \rangle. \quad (6)$$

In the case of inhomogeneous fluids, Eq. (4) becomes⁵¹

$$f_{ac} = -\frac{1}{4} |p_1|^2 \nabla \kappa_0 - \frac{1}{4} |v_1|^2 \nabla \rho_0, \quad (7)$$

where $\kappa_0(r, \tau) = \kappa_0^{(0)} (1 + \hat{\kappa}(r, \tau)) = 1/(\rho_0 c_0^2)$ is the adiabatic compressibility, and p_1 and v_1 are time-harmonic first-order perturbations of acoustic pressure and acoustic velocity, respectively. $\hat{\kappa}(r, \tau)$ is dimensionless compressibility relative deviation from the reference compressibility $\kappa_0^{(0)}$. To obtain simple analytical results, we consider small variations in density ρ_0 and speed of sound c_0 (weakly inhomogeneous limit), i.e., $|\hat{\rho}|, |\hat{c}| \ll 1$. In a weakly inhomogeneous field, it is possible to employ time harmonic first order acoustic fields as $p_1^{(0)}$ and $v_1^{(0)}$ from solutions of homogeneous-fluid wave equation that are known analytically.⁵¹ Consequently, this constitutes a major simplification in acoustic force density expression.

It is important to note here that this approach allows us to simulate the slow-time-scale hydrodynamics in acoustic fields without resolving the fast-acoustic time scale. With acoustic plane standing wave of pressure amplitude p_a and wavenumber $k_\lambda = \frac{2\pi\alpha}{\lambda}$, the incoming first-order acoustic fields in the x direction are given by

$$p_1^{(0)} = p_a \sin(k_\lambda x), \quad (8)$$

$$v_1^{(0)} = \frac{p_a}{i\rho_0^{(0)} c} \cos(k_\lambda x), \quad (9)$$

which together with Eq. (7) leads to Ref. 50

$$f_{ac} = E_{ac}^{(0)} (\cos(2k_\lambda x) \nabla \rho + (1 + \cos(2k_\lambda x)) \nabla \hat{c}), \quad (10)$$

where $E_{ac}^{(0)} = \frac{1}{4} k_0^{(0)} p_a^2$ is the time averaged homogeneous-fluid acoustic energy density inside the channel. This is the principle equation used throughout our work. It is noted that this force is nonzero, if there exist an inhomogeneity in density or velocity of sound. Even though the above theory is valid only in weakly inhomogeneous limits, it is demonstrated experimentally that this acoustic force density Eq. (10) predicts the relocation of fluids accurately even upto 15% density deviation.⁵¹

As already mentioned, the alternating multinode (AMN) standing acoustic wave mixing technique is employed in this study. To implement this, acoustic standing waves of various wavelengths ($\lambda\alpha = W_c$) are used, α corresponds to the number of wavelengths, and W_c is the corresponding channel dimension along the wave direction. $\alpha = 1/2$ corresponds to standing half-wave, and $\alpha = 1$ corresponds to the standing full wave. Similarly, $\alpha = 2, 3$, and 4 correspond to two-wave, three-wave, and four-wave, respectively. The bulk acoustic wave (BAW) microfluidic chip is usually made of hard materials such as silicon and glass. Therefore, acoustic body force is employed in such a way that pressure antinodes will be formed at the walls due to the hard wall boundary condition. The number of nodes N formed in the microchannel for the standing waves of $\alpha = \frac{1}{2}, 1, 2, 3$, and 4 are $N = 1, 2, 3, 4$, and 8 , respectively. The dimension of the channel used in this study is $400 \mu\text{m}$. Consequently, the frequency of the wave, $\omega = c/\lambda$ for $\alpha = \frac{1}{2}, 1, 2$, and 4 are 1.875 MHz , 3.75 MHz , 7.5 MHz , and 15 MHz , respectively. To introduce the chaotic advection, number of nodes and position of nodes are periodically changed by changing the frequencies of the standing waves. Rectangular piecewise functions are formulated for frequencies in such a way to enable generation of alternating standing waves of different wavelengths or number of nodes.

D. Quantification of mixing

Performance of the mixing in this simulation is quantified using mixing index MI,³³ expressed by

$$MI = 1 - \frac{\sigma_i}{\sigma_0}, \text{ where } \sigma_i = \sqrt{\frac{1}{N} \sum_{i=1}^N (\phi_i - \phi_m)^2}, \\ \sigma_0 = \sqrt{\frac{1}{N} \sum_{i=1}^N (\phi_0 - \phi_m)^2}, \quad (11)$$

where σ is the standard deviation of the concentration in a given cross-section, ϕ_i is the point concentration at i th sample point,

ϕ_m is the mean concentration, ϕ_0 is the initial concentration of non-mixed section, and N is the total number of sampling points. As it is evident from the formula, mixing index lies in between 0 and 1, where 0 indicates that fluids are completely unmixed, and 1 indicates complete mixing.

E. Numerical implementation

The system of governing equations (1)–(3) is solved numerically using a finite difference scheme, and acoustic force density Eq. (10) is substituted as a body force term in the Navier-Stokes equation. All the time-dependent mixing studies presented in this work are carried out in a finite element method based solver COMSOL Multiphysics 5.4. This acoustic mixing problem is solved by coupling predefined laminar flow module and dilute species module.

The evolution of the concentration field, velocity field, and density are captured by employing a backward differential formulation with an adaptive timestepping scheme based on local

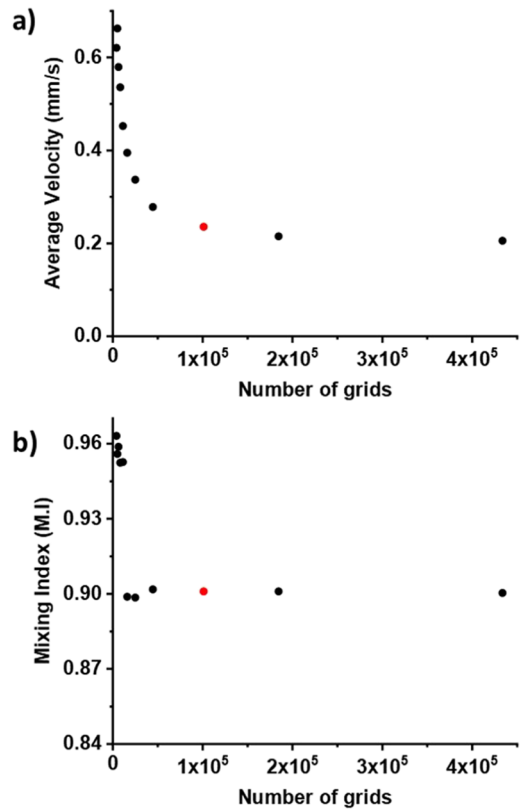


FIG. 2. Convergence plot of the parameters. (a) Mixing Index and (b) average velocity as the number of elements is increased. 3-inlet coflow configuration is used for the convergence test along with the standing acoustic wave propagation direction parallel to the initial fluid-fluid interface ($E_{ac} = 50 \text{ J/m}^3$). The densities of water and iodixanol (20%) are taken as 1005 kg/m^3 and 1110 kg/m^3 , respectively. The red dot indicates the number of grids (101 094) chosen, resulting in a fine computational mesh for above dependent variables to reach convergence.

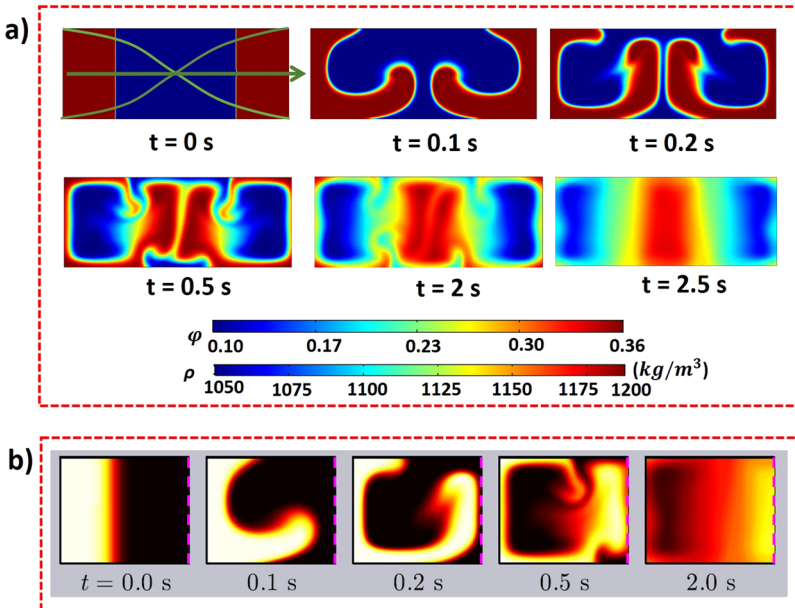


FIG. 3. Time evolution of concentration fields excited by a standing half-wave on a 3-inlet coflow configuration. (a) Obtained relocation result and (b) previously reported result⁵¹ (pink line is the symmetry line and only relocation at the left half is shown). The obtained relocation result at different instants shown is in full agreement with the previously reported results. 10% iodixanol (dark blue) and 36% iodixanol (dark red) solutions are used as low density and high density fluids with $E_{ac} = 10 \text{ J/m}^3$ and the channel dimension of width $W = 375 \mu\text{m}$ and height $H = 150 \mu\text{m}$. Figure 3(b) is adapted from Ref. 51.

error estimates. An initial time step of about 0.1 ms and a maximum step of about 1 ms are used for time-stepping. The choice of maximum timestepping is estimated from the numerical stability criteria, Courant number $\text{Co} = U\Delta t/\Delta x < 1$, where U is the characteristic flow speed ($\sim 0.002 \text{ m/s}$ in our problem), Δt is the timestep, and Δx is the local cell size ($\sim 2 \mu\text{m}$). The time-dependent solver in COMSOL is free to choose a smaller timestep than the given values and automatically adjust the timestep size subject to keep the local error estimates within the desired limits, which is controlled by the user-specified relative tolerance, $R = 0.001$.

Mesh convergence analysis was performed as shown in Fig. 2 to determine the number of grids large enough for all dependent variables to converge ensuring a mesh independent result. The number of triangular grids used is 101 094 (maximum element mesh size of about $2 \mu\text{m}$), beyond which the flow field and concentration field are unaffected with the increase in the number of grids. To our knowledge, the influence of acoustic body force on mixing in microchannels has not been investigated previously. Hence, our analysis is validated by comparing the relocation pattern evolution at different instants with previously reported results.⁵¹ The obtained relocation result shown in Fig. 3(a) is in full agreement with the previously reported results [Fig. 3(b)].

III. RESULTS AND DISCUSSIONS

The following results are aimed at showing a novel mixing process of two fluids in a microchannel by alternating the multinode mixing technique. We investigated the performance of this mixing technique on three different initial flow configurations that we often encounter in microfluidics. We also studied the dependence of the wave propagation direction on mixing performance separately.

A. Acoustic mixing using the alternating multinode (AMN) technique

The mixing of concentration fields in the squared microchannel using the mechanism of alternating multinode (AMN) mixing is demonstrated in this section. In this method, “multinode” and “alternating” are the two important key words. First, multinode standing acoustic waves are used to increase the number of fluid-fluid interfaces or parallel laminations. Increasing the laminations reduces the characteristic mixing length scale, which in turn reduces the mixing time. Second, this method uses ultrasonic standing waves of alternating wavelengths to change the number of nodes and nodal positions periodically to create chaotic advection. Using the acoustic mixing technique, both parallel laminations and chaotic advection are simultaneously generated to achieve rapid mixing, which is the underlying principle of this method. Water-iodoxinal solution is employed as a working fluid in this work. The density of aqueous iodoxinal solution can be varied from 1005 kg/m^3 to 1110 kg/m^3 by varying the concentration of iodoxinal from 0% to 20% (10.4% density difference). The variation in the velocity of sound of the aqueous iodoxinal solution is neglected as it is almost constant (1496 m/s – 1507 m/s) with a maximum relative difference of up to 0.73% for all concentrations of iodoxinal from 0% to 20%. For constant velocity of sound fluid combinations, the acoustic force density Eq. (10) reduces to

$$f_{ac} = E_{ac}(\cos(2k_\lambda x) \nabla \hat{\rho}). \quad (12)$$

Therefore, all the simulation results can be explained only in terms of density. A constant acoustic energy density of about 50 J/m^3 is applied in all simulations. In Fig. 3(a), we consider an initial configuration of the 3-inlet coflowing fluids, where central stream is lighter fluid, sides streams are denser fluid, and the acoustic standing wave of the alternating wavelength is applied parallel to the interface. Inspecting Figs. 4(a) and 4(b), the initial concentration

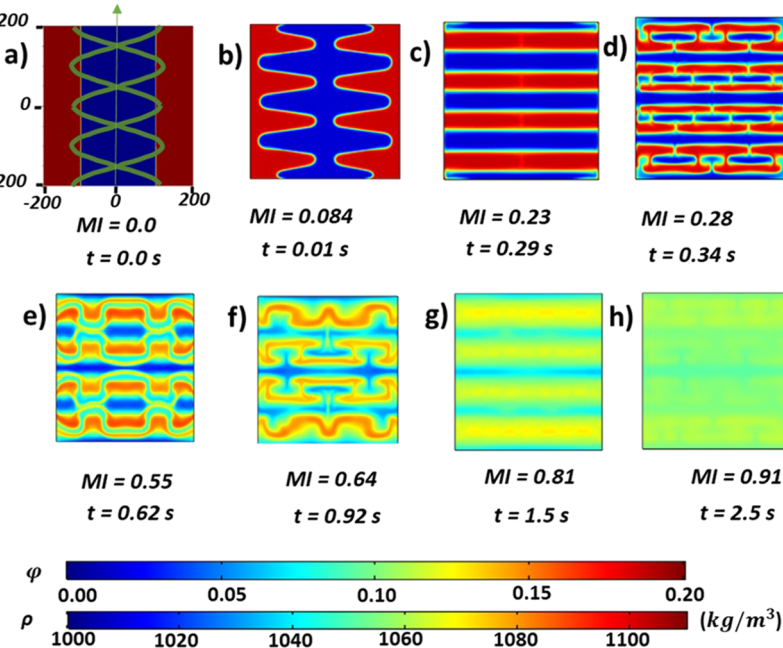


FIG. 4. The time evolution of concentration fields illustrating the acoustic mixing excited by a vertical standing acoustic wave in a direction parallel to the initial fluid-fluid interface. (a) 3-inlet coflow configuration at $t = 0$ s with dense fluid (20% iodixanol, red) located as two vertical slabs at the sides and less dense fluid (0% iodixanol or water, blue) focused at the center. The green colored line represents the standing acoustic wave direction, (b) $t = 0.01$ s (4 nodes), (c) $t = 0.29$ s (4 nodes), (d) $t = 0.34$ s (8 nodes), (e) $t = 0.62$ s (4 nodes), (f) $t = 0.92$ s (8 nodes), (g) $t = 0.81$ s, and (h) $t = 2.5$ s. The colors indicate the density of the concentration field varying from $1005 \text{ kg}/\text{m}^3$ (dark blue) to $1110 \text{ kg}/\text{m}^3$ (dark red) evolving toward a uniform concentration distribution (green) to those of Fig. 4(h). Mixing Index (MI) indicates the degree of mixing in the respective simulation.

field introduces density inhomogeneity, and as a consequence, one finds that the relocation of fluids is engaged as soon as the acoustics is just switched on. This is expected as it has been demonstrated experimentally, theoretically, and numerically that the acoustic fields relocate the higher density fluid portion to nodes and low-density fluid portion to antinodes.⁵¹ This relocation facilitates to increase the number of fluid-fluid interface or parallel laminations as shown in Fig. 4(c). From Fig. 4(c), 4 nodes are produced when the acoustic standing wave of wavelength $200 \mu\text{m}$ is applied in the channel dimension of $400 \mu\text{m}$. It is clear that higher density fluid gets relocated to nodes and four higher density bands in Fig. 4(c) correspond to four nodes. By the use of multinodes, the number of parallel laminations or streams is increased to 4 [Fig. 4(c)] as compared to 2 parallel streams [Fig. 4(a)]. Mixing time scale ($\tau_{mix} \approx \frac{W^2}{n^2 D}$) for n parallel laminations is inversely proportional to n^2 . Hence, the mixing time of the relocated fluid configuration as shown in Fig. 4(c) gets reduced 4 times compared to the mixing time of the initial configuration as shown in Fig. 4(a). After 0.3 s, as shown in Fig. 4(d), the number of nodes is increased to 8 by changing the wavelength of acoustic standing wave to $100 \mu\text{m}$. This produces 8 parallel streams [Fig. 4(d)] compared to 2 parallel streams in initial configuration [Fig. 4(a)]. In this case, the mixing time will be reduced 16 times as compared to the initial configuration. This clearly demonstrates mixing enhancement through increasing parallel laminations by an acoustic relocation phenomenon.

The standing wave wavelength is altered periodically from $200 \mu\text{m}$ to $100 \mu\text{m}$ in a time interval of 0.3 s. This ultrasonic standing waves of alternating wavelengths are employed to change the number of nodes and nodal positions periodically to create chaotic advection. These alternating nodal patterns result in a change in the nodal position, which facilitates high-density and low density fluids to

relocate continuously. Consequently, this produces a fluctuation of flow velocity in time, generating a flow pattern that ultimately results in chaotic advection of the fluid elements. This repeated relocation of fluids by alternating the two frequencies for short time periods in a rectangular piecewise manner produces both parallel lamination and chaotic advection effect. It is evident from Figs. 4(a)–4(h) that the combination of both effects enhances the mixing. A mixing index of about 0.9 (90% mixing) is achieved in about 2.5 s as shown in Fig. 4(h). This marks a significant improvement compared to the mixing without acoustics. We refer the reader to Fig. 5, which shows time-resolved simulation results of a concentration field only due to diffusion (without acoustics). As seen from Fig. 5, diffusion mixing is prolonged and to achieve almost complete mixing ($MI = 0.9$) it takes approximately 100 s for 3-inlet coflow configuration of equal width, 400 s for 2-inlet coflow configuration of equal width, and 364 s for 2-inlet coflow configuration of unequal width. Conversely, employing acoustic force results in more number of fluid-fluid interfaces and strong advection in the domain of interest with high mixing index of about 90% in just 2–3 s as discussed in Sec. II. Clearly, mixing time due to acoustics (~ 2 s) is reduced by two orders of magnitude compared to the mixing (without acoustics) due to diffusion (~ 100 to 400 s).

B. Effect of the wave propagation direction on mixing fluids of different initial flow configurations

Next, for the same initial configuration, the effect of the directional change of standing wave on mixing performance is investigated. In our first problem (Fig. 4), the acoustic field is excited in the vertical y -direction, specifically in the direction parallel to the fluid-fluid interface. Our second problem extends the previous problem by keeping the magnitude of force and initial configuration constant

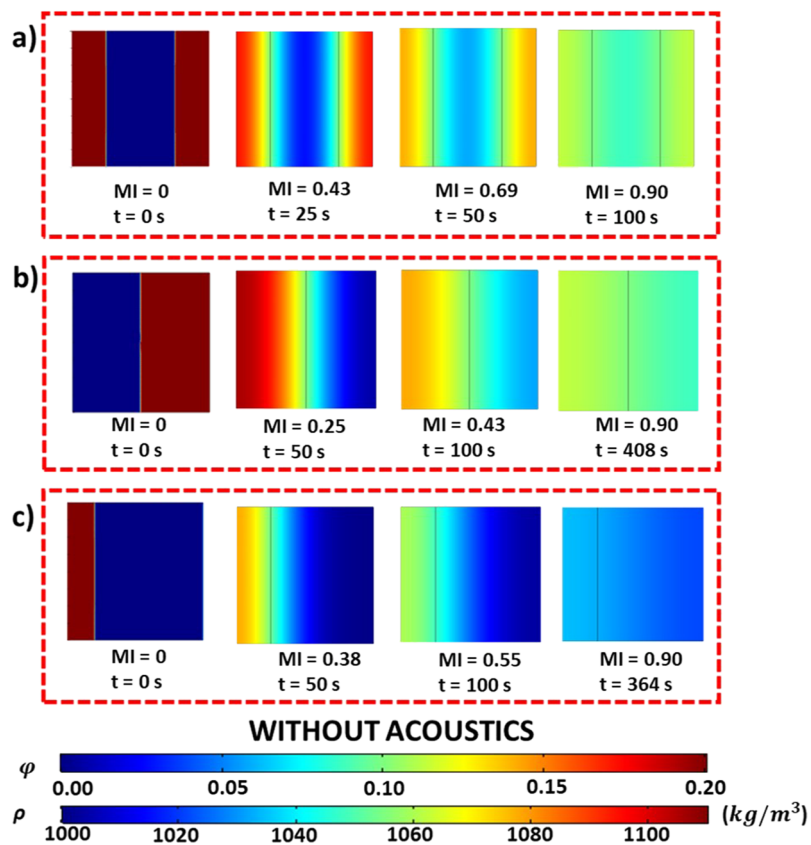


FIG. 5. The time evolution of concentration fields due to diffusion only: (a) 3-inlet coflow system, (b) 2-inlet coflow system of equal width, and (c) 2-inlet coflow system of unequal width.

but is excited by the standing wave acoustic field perpendicular to the initial interface, as shown in Fig. 6. By contrast to the field imposed parallel to the initial interface, the mixing performance is significantly reduced when the acoustic field applied is perpendicular to the

fluid-fluid interface. From Fig. 6, to achieve mixing index $MI = 0.9$, the time taken by the perpendicular acoustic field to mix the fluids is 13.35 s, which is 5 times higher compared to the parallel acoustic field as it only took 2.5 s (Fig. 4). Comparing the fluid mixing

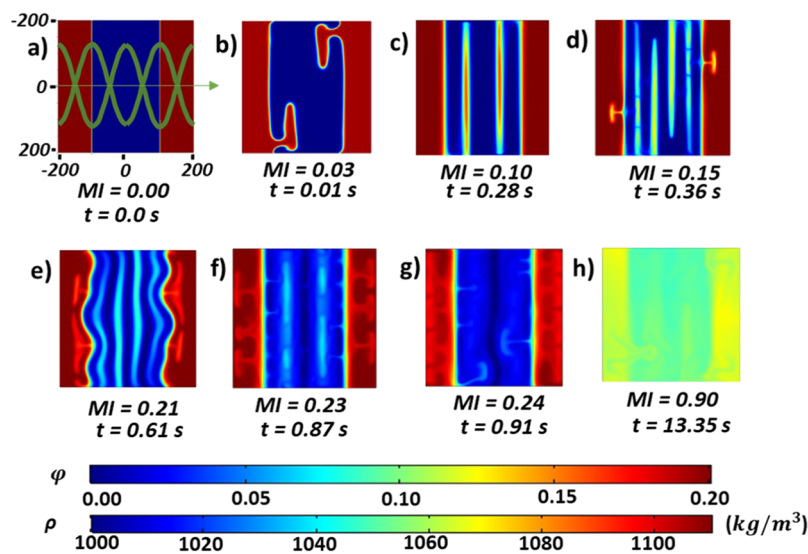


FIG. 6. The time evolution of concentration fields illustrating the acoustic mixing excited by a horizontal standing acoustic wave in a direction perpendicular to the initial fluid-fluid interface. (a) 3-inlet coflow configuration at $t = 0$ s, (b) $t = 0.01$ s (4 nodes), (c) $t = 0.28$ s (4 nodes), (d) $t = 0.36$ s (8 nodes), (e) $t = 0.61$ s (4 nodes), (f) $t = 0.87$ s (4 nodes), (g) $t = 0.91$ s, and (h) $t = 13.35$ s.

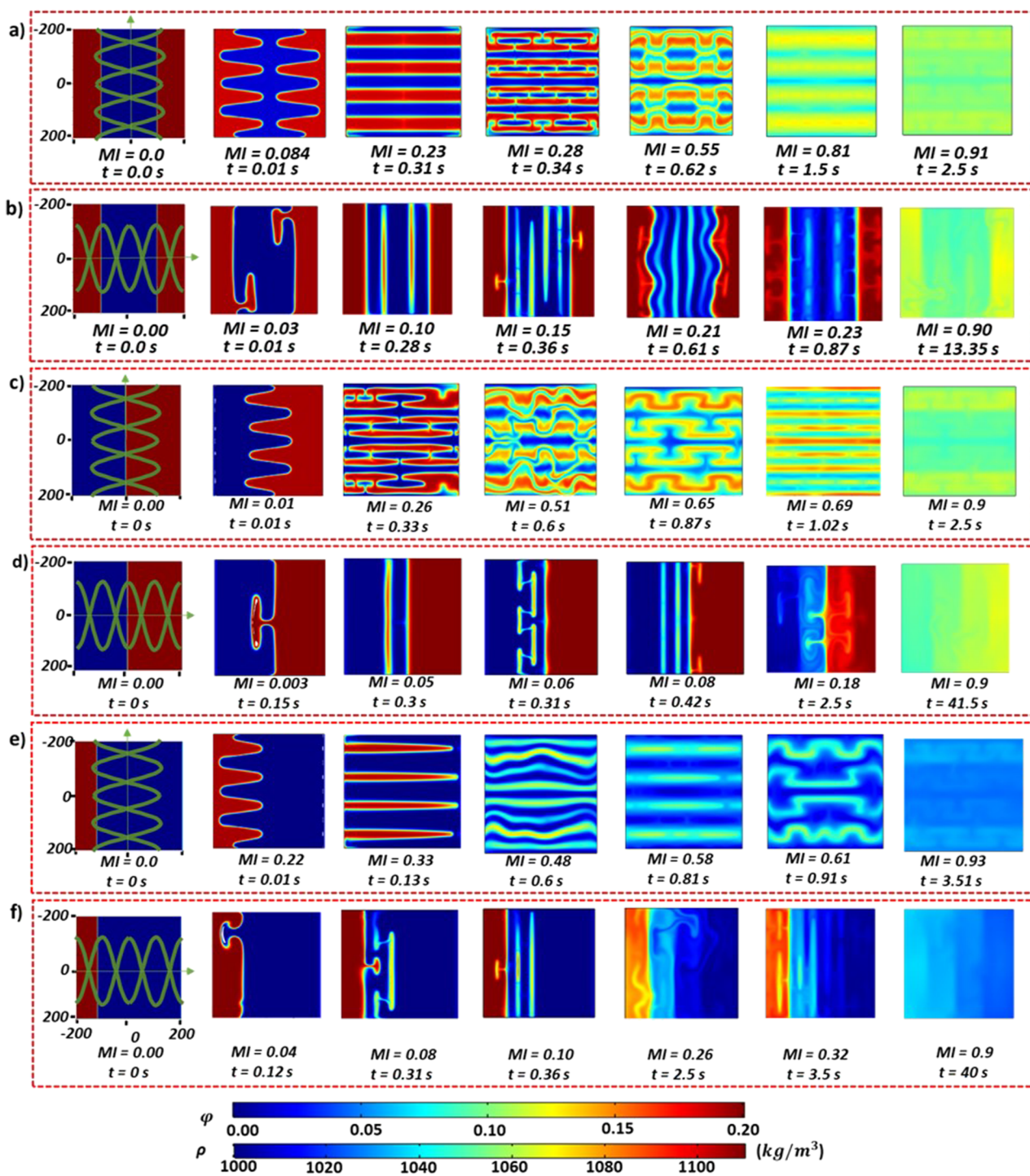


FIG. 7. Concentration profiles of iodixanol solutions illustrating the effect of initial configuration and the direction of standing wave on mixing. The rows [(a)–(f)] correspond to the six cases, combinations of different initial configurations, and direction of the standing wave. (a) 3-inlet coflow system with wave direction parallel to the interface, (b) 3-inlet coflow system with wave direction perpendicular to the interface, (c) 2-inlet system coflow of equal width with wave direction parallel to the interface, (d) 2-inlet coflow system of equal width with wave direction perpendicular to the interface, (e) 2-inlet coflow system of unequal width with wave direction parallel to the interface, and (f) 2-inlet coflow system of unequal width with wave direction perpendicular to the interface. All plots show marked variations in Mixing time (t) and Mixing Index (MI) evolving to the end configuration of 0.9 MI.

by the parallel acoustic field shown in Fig. 4 with the perpendicular acoustic field shown in Fig. 6, it is particularly evident that acoustic fields applied parallel to the fluid-fluid interface relocate inhomogeneous fluids properly and evenly, which facilitated proper parallel lamination, whereas the acoustic field applied perpendicular to the interface does not relocate fluids properly and resulted in poor and uneven parallel lamination.

In general, one would expect different mixing behavior on different initial configurations, when the acoustic fields of different directions are imposed. To enhance the understanding of mixing effects in the two-fluid system using the AMN technique, the evolution of the solute concentration field for different initial flow configurations is investigated. To establish the generality of this AMN technique, in our study, we consider three different initial flow configurations commonly used in microfluidics as shown in Fig. 1, namely, 3-inlet coflow configuration, 2-inlet coflow configuration of equal width, and 2-inlet coflow configuration of unequal width. Simulation results for the acoustic mixing at various time instants for different microchannel flow configurations are illustrated in Fig. 7. The distinct mixing patterns are observed for different initial configurations when the acoustic standing waves of different directions are applied. 3-inlet coflow configuration results from Figs. 4 and 6 are mentioned again in Figs. 7(a) and 7(b) to improve the readability. The time taken by the acoustic field parallel to the interface to mix the fluids in different flow configurations is approximately same, 2.5 s–3.5 s, for the given MI 0.9 as shown in Figs. 7(a), 7(c), and 7(e). Whereas, for the acoustic field perpendicular to the interface as shown in Figs. 7(b), 7(d), and 7(f), the mixing time required to achieve $MI = 0.9$ is 13.35 s for the 3-inlet coflow configuration, 41.5 s for 2-inlet coflow configuration of equal width, and 40 s for 2-inlet coflow configuration of unequal width. By comparing Figs. 5 and 7, in the case of 3-inlet coflow configuration, the acoustic field applied parallel to the interface mixes the fluids in 2.5 s, acoustic field applied perpendicular to the interface mixes the fluids in 13.35 s, and it takes 100 s for mixing of the fluids due to diffusion without using acoustics. Similarly, in the case of 2-inlet coflow configuration of equal width, the acoustic field applied parallel to the interface mixes the fluids in 2.5 s, acoustic field applied perpendicular to interface mixes the fluids in 41.5 s, and it takes

400 s for mixing of the fluids due to diffusion without using acoustics. Again, in the case of 2-inlet coflow configuration of unequal width, the acoustic field applied parallel to the interface mixes the fluids in 3.51 s, acoustic field applied perpendicular to the interface mixes the fluids in 40 s, and it takes 364 s for mixing of the fluids due to diffusion without using acoustics. Hence, we have shown that the acoustic field parallel to the interface reduces the mixing time by approximately two order of magnitude compared with the mixing without acoustics, whereas the acoustic field applied perpendicular to the interface reduces the mixing time by approximately one order of magnitude compared to the mixing without acoustics.

The simulation results shown in Fig. 7 clearly suggest that the acoustic wave propagated parallel to the interface mixes the fluids more effectively (in less time) compared to the acoustic wave perpendicular to the interface. The reason for this surprising and remarkable result follows. As discussed earlier, if there is any inhomogeneity in density present between two nodes or antinodes, then the high-density fluid will be relocated to the nodes or low-density fluid will be relocated to the antinodes. If fluid is homogeneous then no relocation is possible. When the acoustic wave is propagated perpendicular to the interface, as shown in Fig. 8(a-1), most of the nodes(N) or antinodes(AN) in the fluid domain do not contain density inhomogeneity between them except only at the central antinode(AN), where slight relocation is observed, as shown in Figs. 8(a-2) and 8(a-3). Therefore, the relocation of fluids is inhibited, which results in the absence of multilayer laminations or improper laminations, as shown in Fig. 8(a-4). Whereas, when the acoustic wave is applied parallel to the interface as shown in Fig. 8(b-1), every single node and antinode contains inhomogeneous fluid between them or in contact with both high-density fluid and low-density fluid as shown in Figs. 8(b-2) and 8(b-3). This results in proper relocation of fluids and formation of multilayer laminations, as shown in Fig. 8(b-4). The above reason clearly explains why the acoustic wave propagated parallel to the fluid-fluid interface is more effective in mixing fluids as compared to the wave perpendicular to the interface. Mixing time can be further reduced for all configurations by optimizing the time interval between the alternating wavelengths.

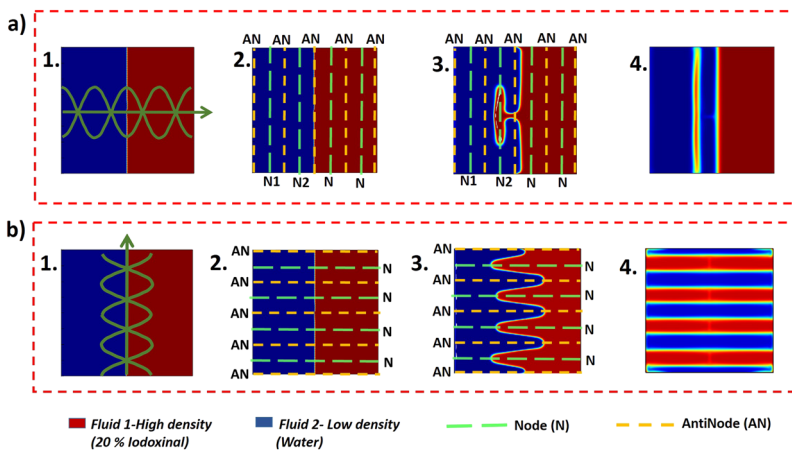


FIG. 8. Plots of concentration distribution of coflow 2-inlet configuration evolving with time illustrating the effect of acoustic field propagating direction on mixing: (a) standing wave perpendicular to the interface and (b) standing wave parallel to the interface. Green dotted lines indicate the node, whereas yellow dotted lines indicate the antinodes of the applied standing acoustic waves.

C. Effect of number of nodes on mixing performance

Finally, the effect of number of nodes (or frequency) of the standing wave on the mixing performance is analyzed. This effect is well illustrated by the scatter plot of the mixing index against time for different number of alternating nodes N and change in directions as shown in Fig. 9. The plots consider the cases of three different configuration systems where the mixing index MI (%) is plotted for different number of nodes and standing wave propagation direction. As discussed in Sec. III B, it is evident from the plots that rapid mixing is achieved in lesser time when the direction of propagation of the wave is parallel to the initial fluid interface. With respect to the number of nodes used, these results show that for a given wave propagation direction, better mixing performance is achieved when number of nodes is switched between $N = 8$ and $N = 4$ (red and blue dots) at regular time intervals when compared to nodes between $N = 4$ and $N = 2$ (black, green dots). This demonstrates the number of nodes as an essential parameter for adequate mixing as higher number of nodes results in better overall mixing. It is obvious that more number of nodes produces more number of parallel laminations or fluid-fluid interfaces, which decreases mixing time significantly by decreasing the striation mixing length.

The main limitation in employing the large arbitrary number of nodes is the thickness of the PZT transducer. To produce more number of nodes, the standing wave of higher frequency (lesser wavelength) has to be employed, which requires thinner PZT plates. For example, to produce 8 nodes in the microchannel dimension of $400 \mu\text{m}$ filled with water ($c = 1495 \text{ m/s}$), the frequency of the applied wave must be around 15 MHz. To generate 15 MHz, the lead zirconate titanate PZT transducer thickness must be around 0.133 mm, which is the least commercially available thick lead zirconate titanate PZT plate in the market. This is the reason for not using more than 8 nodes or 15 MHz frequency for channel dimension $400 \mu\text{m}$ used in this work. However, thick and thin PZT films (100 nm to $100 \mu\text{m}$) deposited on the substrate can overcome these limitations.

Fluid retention time is given as $t_{ch} = \frac{L_{ch}}{U}$, where L_{ch} is the channel length and U is the characteristic axial flow velocity. If the mixing time t_{mix} is less than or equal to the retention time ($t_{mix} \leq t_{ch}$), then fluid mixing will be complete. The mixing time predicted from the 2D simulation does not exactly match with the mixing time required for the actual flow in the 3D channel due to the nonuniform velocity profile with peak velocity U_p at the center and zero velocity at the walls. However, this limitation is not of great importance, as in practice the mixing time obtained from 2D simulation can be used to predict the upper limit or maximum allowable flow rate (Q_{max}) in which fluid is being sent through the 3D microchannel, such that the fluid mixing is complete for the given channel length. This is done by taking characteristic flow velocity U as peak velocity U_p . Hence, for complete mixing, $t_{mix} \leq \frac{L_{ch}}{U_p}$. Consequently,

$Q_{max} = \frac{A \cdot L_{ch}}{t_{mix}}$ can be calculated from the t_{mix} obtained from 2D simulation. For the system under consideration, with cross-sectional area $A = 0.16 \text{ mm}^2$, mixing time $t_{mix} \approx 2 \text{ s}$, and typical downstream channel length $L = 2 \text{ cm}$, Q_{max} is calculated as $96 \mu\text{l/min}$, which is in the same order of typical flow rates encountered in the microchannel.

It is quite evident from Eq. (10) that weaker inhomogeneity in density and speed of sound leads to weaker acoustic force

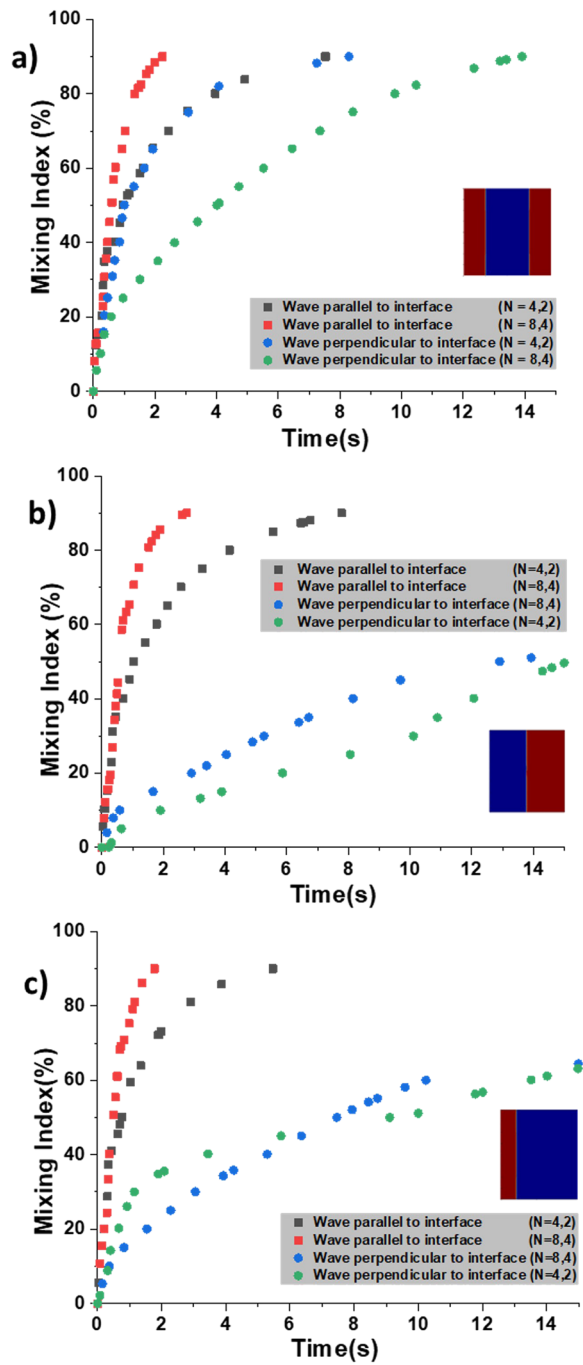


FIG. 9. Scatter plots illustrating the mixing performance for different initial configurations, number of nodes, and wave directions: (a) 3-inlet coflow system, (b) 2-inlet coflow system of equal width, and (c) 2-inlet coflow system of unequal width. All the results have the same imposed acoustic energy density of 50 J/m^3 .

density, which results in longer mixing time. To understand the effect of initial density variation on mixing time, simulations of three different density deviations (10.8%, 1.1%, and 0.5%) are performed as shown in Fig. 10. When the density variation is reduced 10 times

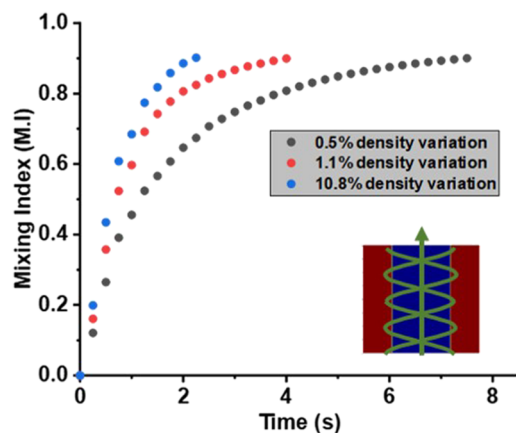


FIG. 10. Scatter plot illustrating the effect of density variations on mixing time to achieve a 0.9 MI for a 3-inlet coflow system. Alternating multinode standing wave between $N = 4$ and $N = 8$ is applied with $E_{ac} = 50 \text{ J/m}^3$.

from 10.8% to 1.1%, the mixing time to achieve 0.9 MI is increased to 4 s from 2.5 s. Similarly, when the density variation is reduced to 0.5%, the mixing time gets increased to 7.5 s. It is clearly seen that the effect of initial density variations on mixing performance at higher density variation results in shorter mixing time as anticipated.

The important limitation of this mixing method based on acoustic relocation phenomenon is, for the acoustic body force that is responsible for relocation to exist, the fluids must be inhomogeneous or must have difference in densities or velocity of sound. Most of the fluids or reagents that we encounter in chemical or biological assays are inhomogeneous and easily fulfill the above requirement. Even if the fluids have same densities or velocity of sound, it is easy to make them inhomogeneous by adding other density modifier agents, without affecting the assay performance. From scaling analysis, it is shown that the density (or velocity of sound) difference of 0.1% is enough to relocate the fluids in a typical microchannel using acoustic body force.⁵¹ Also, this relocation phenomenon is experimentally demonstrated to occur even with 1% percentage density difference or velocity of sound difference. From the above facts it is evident that this limitation can be easily tackled.

IV. CONCLUSIONS

We have presented theoretical validation and simulation results of the newly proposed acoustic mixing method in microchannels based on the relocation phenomenon. Acoustic mixing is achieved via an alternating multinode (AMN) method by periodically switching the nodal positions and number of nodes of the applied standing acoustic wave. The sensitivity of this method is high enough to drastically reduce the mixing time and improve the mixing quality from typical methods. A systematic study over the wave propagation direction, different initial flow configurations, and number of nodes was performed to illustrate the effects of different parameters on mixing time. From the results, we can conclude that the viable route for rapid and efficient mixing in a microchannel is achieved

when multinode standing waves are applied in the direction parallel to the initial fluid-fluid interface irrespective of initial flow configurations. Future development area can apply this proposed idea on multi-inlet channel systems. Further validation studies to compare the numerical methods directly with experimental results would be interesting to investigate. To refine the work further, the effects of different relevant parameters such as acoustic energy density and velocity of sound on mixing performance should be investigated.

REFERENCES

- ¹H. Pennemann, V. Hessel, and H. Löwe, "Chemical microprocess technology—From laboratory-scale to production," *Chem. Eng. Sci.* **59**, 4789–4794 (2004).
- ²V. Hessel and H. Löwe, "Microchemical engineering: Components, plant concepts user acceptance—Part I," *Chem. Eng. Technol.* **26**, 13–24 (2003).
- ³L. Dul'neva and A. Moskvin, "Kinetics of formation of peroxyacetic acid," *Russ. J. Gen. Chem.* **75**, 1125–1130 (2005).
- ⁴A. de Mello and R. Wootton, "But what is it good for? Applications of microreactor technology for the fine chemical industry. Review developments in microreactor technology," *Lab Chip* **2**, 7N–13N (2002).
- ⁵G. S. Jeong, S. Chung, C.-B. Kim, and S.-H. Lee, "Applications of micromixing technology," *Analyst* **135**, 460–473 (2010).
- ⁶V. Hessel, H. Löwe, and S. Hardt, *Chemical Micro Process Engineering: Fundamentals, Modelling and Reactions* (John Wiley & Sons, 2004), Vol. 1.
- ⁷W. Ehrfeld, V. Hessel, and H. Löwe, *Microreactors: New Technology for Modern Chemistry* (Wiley, 2000).
- ⁸G. Whitesides, "The lab finally comes to the chip!," *Lab Chip* **14**, 3125–3126 (2014).
- ⁹W. Snyder, Y.-S. Han, G. Bilbro, R. Whitaker, and S. Pizer, "Image relaxation: Restoration and feature extraction," *IEEE Trans. Pattern Anal. Mach. Intell.* **17**, 620–624 (1995).
- ¹⁰N.-T. Nguyen and Z. Wu, "Micromixers—A review," *J. Micromech. Microeng.* **15**, R1 (2004).
- ¹¹V. Hessel, H. Löwe, and F. Schönfeld, "Micromixers—A review on passive and active mixing principles," *Chem. Eng. Sci.* **60**, 2479–2501 (2005).
- ¹²K. Ward and Z. H. Fan, "Mixing in microfluidic devices and enhancement methods," *J. Micromech. Microeng.* **25**, 094001 (2015).
- ¹³M. A. Ansari and K.-Y. Kim, "Mixing performance of unbalanced split and recombine micromixers with circular and rhombic sub-channels," *Chem. Eng. J.* **162**, 760–767 (2010).
- ¹⁴A. D. Stroock, S. K. Dertinger, G. M. Whitesides, and A. Ajdari, "Patterning flows using grooved surfaces," *Anal. Chem.* **74**, 5306–5312 (2002).
- ¹⁵A. E. Kamholz, B. H. Weigl, B. A. Finlayson, and P. Yager, "Quantitative analysis of molecular interaction in a microfluidic channel: The t-sensor," *Anal. Chem.* **71**, 5340–5347 (1999).
- ¹⁶R. H. Liu, M. A. Strempler, K. V. Sharp, M. G. Olsen, J. G. Santiago, R. J. Adrian, H. Aref, and D. J. Beebe, "Passive mixing in a three-dimensional serpentine microchannel," *J. Microelectromech. Syst.* **9**, 190–197 (2000).
- ¹⁷V. Mengeaud, J. Josserand, and H. H. Girault, "Mixing processes in a zigzag microchannel: Finite element simulations and optical study," *Anal. Chem.* **74**, 4279–4286 (2002).
- ¹⁸Y. Wu, Y. Ren, Y. Tao, L. Hou, Q. Hu, and H. Jiang, "A novel micromixer based on the alternating current-flow field effect transistor," *Lab Chip* **17**, 186–197 (2017).
- ¹⁹T. Zhou, H. Wang, L. Shi, Z. Liu, and S. Joo, "An enhanced electroosmotic micromixer with an efficient asymmetric lateral structure," *Micromachines* **7**, 218 (2016).
- ²⁰M. Jalal, B. Khorshidi, and E. Esmaeilzadeh, "Electrohydrodynamic (EHD) mixing of two miscible dielectric liquids," *Chem. Eng. J.* **219**, 118–123 (2013).
- ²¹D. T. Kumar, Y. Zhou, V. Brown, X. Lu, A. Kale, L. Yu, and X. Xuan, "Electric field-induced instabilities in ferrofluid microflows," *Microfluid. Nanofluid.* **19**, 43–52 (2015).

- ²²G. Wang, F. Yang, and W. Zhao, "There can be turbulence in microfluidics at low Reynolds number," *Lab Chip* **14**, 1452–1458 (2014).
- ²³Q. Xia and S. Zhong, "Liquid mixing enhanced by pulse width modulation in a y-shaped jet configuration," *Fluid Dyn. Res.* **45**, 025504 (2013).
- ²⁴Y. Abbas, J. Miwa, R. Zengerle, and F. von Stetten, "Active continuous-flow micromixer using an external Braille pin actuator array," *Micromachines* **4**, 80–89 (2013).
- ²⁵M. Du, Z. Ma, X. Ye, and Z. Zhou, "On-chip fast mixing by a rotary peristaltic micropump with a single structural layer," *Sci. China: Technol. Sci.* **56**, 1047–1054 (2013).
- ²⁶C. A. Cortes-Quiroz, A. Azarbadeegan, I. D. Johnston, M. C. Tracey *et al.*, "Analysis and design optimization of an integrated micropump-micromixer operated for bio-MEMS applications," in Proceedings of the 4th Micro and Nano Flows Conference, London, UK, 7–10 September 2014, pp. 261–271.
- ²⁷D. Nouri, A. Zabihi-Hesari, and M. Passandideh-Fard, "Rapid mixing in micromixers using magnetic field," *Sens. Actuators, A* **255**, 79–86 (2017).
- ²⁸M. La, W. Kim, W. Yang, H. W. Kim, and D. S. Kim, "Design and numerical simulation of complex flow generation in a microchannel by magnetohydrodynamic (MHD) actuation," *Int. J. Precis. Eng. Manuf.* **15**, 463–470 (2014).
- ²⁹M. Chang, J. L. F. Gabayno, R. Ye, K.-W. Huang, and Y.-J. Chang, "Mixing efficiency enhancing in micromixer by controlled magnetic stirring of Fe₃O₄ nanomaterial," *Microsyst. Technol.* **23**, 457–463 (2017).
- ³⁰Q. Cao, X. Han, and L. Li, "An active microfluidic mixer utilizing a hybrid gradient magnetic field," *Int. J. Appl. Electromagn. Mech.* **47**, 583–592 (2015).
- ³¹D. Owen, M. Ballard, A. Alexeev, and P. J. Hesketh, "Rapid microfluidic mixing via rotating magnetic microbeads," *Sens. Actuators, A* **251**, 84–91 (2016).
- ³²A. Ozcelik, D. Ahmed, Y. Xie, N. Nama, Z. Qu, A. A. Nawaz, and T. J. Huang, "An acoustofluidic micromixer via bubble inception and cavitation from microchannel sidewalls," *Anal. Chem.* **86**, 5083–5088 (2014).
- ³³H. Van Phan, M. B. Coşkun, M. Şen, G. Pandraud, A. Neild, and T. Alan, "Vibrating membrane with discontinuities for rapid and efficient microfluidic mixing," *Lab Chip* **15**, 4206–4216 (2015).
- ³⁴S. Orbay, A. Ozcelik, J. Lata, M. Kaynak, M. Wu, and T. J. Huang, "Mixing high-viscosity fluids via acoustically driven bubbles," *J. Micromech. Microeng.* **27**, 015008 (2016).
- ³⁵P.-H. Huang, Y. Xie, D. Ahmed, J. Rufo, N. Nama, Y. Chen, C. Y. Chan, and T. J. Huang, "An acoustofluidic micromixer based on oscillating sidewall sharp-edges," *Lab Chip* **13**, 3847–3852 (2013).
- ³⁶C. Huang and C. Tsou, "The implementation of a thermal bubble actuated microfluidic chip with microvalve, micropump and micromixer," *Sens. Actuators, A* **210**, 147–156 (2014).
- ³⁷G. Kunti, A. Bhattacharya, and S. Chakraborty, "Rapid mixing with high-throughput in a semi-active semi-passive micromixer," *Electrophoresis* **38**, 1310–1317 (2017).
- ³⁸A. Wixforth, "Acoustically driven planar microfluidics," *Superlattices Microstruct.* **33**, 389–396 (2003).
- ³⁹K. Sritharan, C. Strobl, M. Schneider, A. Wixforth, and Z. Guttenberg, "Acoustic mixing at low Reynold's numbers," *Appl. Phys. Lett.* **88**, 054102 (2006).
- ⁴⁰R. H. Liu, J. Yang, M. Z. Pindera, M. Athavale, and P. Grodzinski, "Bubble-induced acoustic micromixing," *Lab Chip* **2**, 151–157 (2002).
- ⁴¹D. Ahmed, X. Mao, J. Shi, B. K. Juluri, and T. J. Huang, "A millisecond micromixer via single-bubble-based acoustic streaming," *Lab Chip* **9**, 2738–2741 (2009).
- ⁴²T. Frommelt, M. Kostur, M. Wenzel-Schäfer, P. Talkner, P. Hänggi, and A. Wixforth, "Microfluidic mixing via acoustically driven chaotic advection," *Phys. Rev. Lett.* **100**, 034502 (2008).
- ⁴³A. Toegl, R. Kirchner, C. Gauer, and A. Wixforth, "Enhancing results of microarray hybridizations through microagitation," *J. Biomol. Tech.* **14**, 197 (2003).
- ⁴⁴H. Ahmed, J. Park, G. Destgeer, M. Afzal, and H. J. Sung, "Surface acoustic wave-based micromixing enhancement using a single interdigital transducer," *Appl. Phys. Lett.* **114**, 043702 (2019).
- ⁴⁵J. Nam and C. S. Lim, "Micromixing using swirling induced by three-dimensional dual surface acoustic waves (3D-dSAW)," *Sens. Actuators, B* **255**, 3434–3440 (2018).
- ⁴⁶W. Qiu, J. T. Karlsen, H. Bruus, and P. Augustsson, "Experimental characterization of acoustic streaming in gradients of density and compressibility," *Phys. Rev. Appl.* **11**, 024018 (2019).
- ⁴⁷J. T. Karlsen, W. Qiu, P. Augustsson, and H. Bruus, "Acoustic streaming and its suppression in inhomogeneous fluids," *Phys. Rev. Lett.* **120**, 054501 (2018).
- ⁴⁸P. Augustsson, J. T. Karlsen, H.-W. Su, H. Bruus, and J. Voldman, "Iso-acoustic focusing of cells for size-insensitive acousto-mechanical phenotyping," *Nat. Commun.* **7**, 11556 (2016).
- ⁴⁹S. Deshmukh, Z. Brzozka, T. Laurell, and P. Augustsson, "Acoustic radiation forces at liquid interfaces impact the performance of acoustophoresis," *Lab Chip* **14**, 3394–3400 (2014).
- ⁵⁰J. T. Karlsen and H. Bruus, "Acoustic tweezing and patterning of concentration fields in microfluidics," *Phys. Rev. Appl.* **7**, 034017 (2017).
- ⁵¹J. T. Karlsen, P. Augustsson, and H. Bruus, "Acoustic force density acting on inhomogeneous fluids in acoustic fields," *Phys. Rev. Lett.* **117**, 114504 (2016).